J Nanostruct 15(4): 1820-1832, Autumn 2025

RESEARCH PAPER

Characterization and Determination of Residual Stresses in Laminated Aluminum Alloy/Epoxy-TiO_2 NPs Composites Using X-ray Technique

*Zahraa B. Latif *, Najim A. Saad, Ammar E. Alkawaz*

College of Material Engineering, University of Babylon, Iraq

ARTICLE INFO

Article History:
Received 03 June 2025
Accepted 03 September 2025
Published 01 October 2025

Keywords:
Aluminum alloy
Deposition Temperature
Laminated Materials
Residual Stress
TiO_2 NPs

ABSTRACT

The residual stresses within the laminated Aluminum metal alloy/epoxy-TiO_2 NPs composites were investigated. Residual stresses play a significant role in the properties and performance of laminated metal alloys/epoxy composites coatings. In this paper, the structural (FE-SEM, XRD and EDS), mechanical (tensile strength) and residual stresses using X-ray technique studied for pure epoxy at different curing temperature (20, 50 and 75 °C) and epoxy reinforced with TiO_2 NPs at different weight ratios (2, 4 and 6 wt. %) as coating materials deposited on Al alloy substrates using spin coating technique. The structural characterizations (FE-SEM and XRD) proved the homogeneous and uniform epoxy coatings with thickness about (240 µm). The obtained results revealed notable differences in residual stresses values depend on the curing temperature and the added TiO_2 NPs content of the epoxy coatings. The pure epoxy coatings exhibited the higher residual stresses values, while the enhanced epoxy coatings with TiO_2 NPs showed the lowest values. The epoxy coatings deposited at (25 °C) and at (2 wt. %) added TiO_2 NPs recorded the highest tensile strength values. The results demonstrated that the adding of TiO_2 NPs to the epoxy coatings enhance the final performance of the coatings. The deposition temperature effect demonstrated that the epoxy coatings cured at high temperatures (75 °C) exhibited high residual stresses values compared to the coatings cured at lower temperature (25 °C).

How to cite this article
Latif Z., Saad N., Alkawaz A. Characterization and Determination of Residual Stresses in Laminated Aluminum Alloy/Epoxy-TiO_2 NPs Composites Using X-ray Technique. J Nanostruct, 2025; 15(4):1820-1832. DOI: 10.22052/JNS.2025.04.030

INTRODUCTION

Residual stresses are those stresses locked into the material even when it is free from external forces. Fabricating processes, thermal processing, welding, and heat treatment, mechanical forming, and extrusion are the most common sources of residual stresses. The residual stresses during cure can have a significant effect on the mechanical properties by inducing warpage or initiating matrix cracks and delamination [1]. It is thus important to prediction and measurement of process-induced residual stresses because a total elimination of residual stresses is hardly ever possible. The measurement of stress in a coating with a thickness of only several micrometers, which includes various phases that differ in their properties, presents a certain challenge. Meanwhile, residual stress has a significant effect on the functional properties of the coatings, their service life periods, and the reliability of the operation of coated products. In particular, cracks and

* *Corresponding Author Email: Zahrabasemlatif@gmail.com*

interlayer delamination can form in the coatings, which leads to the destruction of the structure, to chipping, and to the loss of functional properties. Compressive stress usually leads to the formation of delamination and longitudinal cracks [2-4], whereas tensile stress leads to the formation of transverse cracks [5,6]. The distribution of residual stress in the coating affects both the adhesion to the substrate and the fracture toughness [7,8,9]. Various defects on the surface of the substrate (micropores, cracks, irregularities, dirt spots, etc.) [10-13] as well as defects in the coating itself (microdroplets, interlayer delamination, etc.) have a significant influence on the coating formation process [11, 12,14].

Epoxy coatings consisting of two components, a base and a hardener, are employed for many applications. However, a range of factors, including intrinsic characteristics, thermal influences, volumetric changes, and lattice disparities, can introduce residual stress into these epoxy coatings, [15]. Due to the mismatch in coefficient of thermal expansion of the resin and a hardener material or additions such as filler, fibers and glass-flake the two materials base and hardener shrink with a different rate and thus introduce residual stresses [16,17]. It is well known that epoxy resins are brittle and show poor resistance to crack initiation and crack propagation. For these reasons, in recent years, research activities have been focused on techniques to improve the fracture resistance (toughness and brittleness) of epoxy resins. One of the most studied techniques consists to incorporate inorganic nanoparticles into the polymer matrix, such as titanium dioxide (TiO_2), alumina (Al_2O_3), silica (SiO_2), carbon black, nanoclays, carbon nanotubes (CNTs) and others [18]. The resulting nanocomposites can exhibit improved thermal, mechanical (including toughness), rheological, electrical and optical properties, among others, even with very low nanofiller contents.

Various methods are used to determine the stress in the coating structure [19]. Most of the experimental methods include the layer removal method, neutron diffraction and the X-ray diffraction (XRD) [20]. Some of these methods are destructive and some are nondestructive. Among the above-mentioned methods, XRD is a technique with high accuracy and nondestructive characteristics, and hence is one of the best choices and convenient tools for the measuring of surface residual stresses. In the X-ray diffraction, the strain in the crystal lattice is measured and the associated residual stress is determined from the elastic constants assuming a linear elastic distortion of the crystal lattice plane [21]. Residual stress evolution in epoxy coatings has been a small area of researches. D. Taisei, et al. (2015) [22] measured the residual stress in polyamide film polymer using the X-ray diffraction technique. The diffractometer with a transmission method was used in experimental measurement. They discussed the problems related to measuring residual stresses in polymer coatings and showed that the X-ray technique is a good method to measure residual stresses in polymer coatings. Mamoon (2021) [23] studied the effects of added nano particles on the mechanical properties of MMNC. Used Aluminum alloy 6061 and 6082 as base material to the Aluminum matrix nano composites (AMNC) and different Titanium Dioxide (TiO_2) nano particles reinforcement wt. % of Ti(0.5, 1.0, 1.5 and 2.0), by using stir casting method. The results indicated improve in the mechanical properties. Observed that the nanomaterial reinforcement led to high improvement in ultimate strength (σu), yield stress (σy), hardness (BHN) and ductility. Hassan, S.R., et al. (2024) [24] measured the residual stresses in combination of silicon carbide substrate and aluminium oxide (SiC-5wt.% Al_2O_3) used as the wear protection coating specifically in wear protection coating, using the $\sin^2\psi$ based on the X-ray diffraction technique. Measured the diffraction angle, 2θ, experimentally, and the lattice spacing is calculated using Bragg's Law using the measured diffraction angle and the known X-ray wavelength. They prove that the X-ray diffraction method is a feasible tool to evaluate and analyse the residual stresses distributions in composite wear protection coating units. The present study concentrated on the characterization and determination of the structural, mechanical and residual stresses for laminated materials consist of Al alloys coated with epoxy resin and study the effect of deposition temperature and the addition of TiO_2 NPs on the prepared laminated materials properties, the X-ray diffraction technique used to determine and investigate the residual stresses within the prepared samples.

MATERIALS AND METHODS

Used Materials

The epoxy Sikadur 52 produced by Sika USA

company with its hardener used in this work as coating material, the epoxy has a transparent color while the hardener brownish color, the density of purchased epoxy of (1.06 Kg/l). The aluminum alloy 6061 used as substrates in present work purchased from Tanc Gang company with purity of (97 %) that widely used in various industry applications, Fig. 6 and Table 1 present the Aluminium alloy composition obtained from EDX exam. The enhancement titanium oxide nanoparticles TiO_2 NPs purchased from SkySpring Nanomaterials, Inc, with purity of (99.5 %) and average particle size of (30 nm) were used without any purification.

Laminated Samples Preparation

The Aluminum A6061 with dimensions of (3×3 cm) and thickness of (6 mm) were polished and cleaned to be used as substrates, the substrates dimensions are considered according to ASTM-E0915-96R02 [25]. Two groups of epoxy coatings have been used in this study. The first group includes pure epoxy coatings which consist of two parts base and hardener in the liquid state, the base and the hardener mixed carefully together in volume ratio (1:2) before being applied to the A6061 aluminum substrates surface at different deposition temperature (25, 50 and 75 °C) using the spin coating technique. The second group included the prepared pure epoxy enhanced with different weight ratio (2, 4 and 6 wt. %) of titanium oxide nanoparticles TiO_2 NPs deposited on the A6061aluminum substrates using spin coating technique. The prepared laminated samples are ready for testing and analyzing. Fig. 1A, B, C presents the Aluminum A6061 substrates before coating, laminated samples coated with pure epoxy, laminated samples coated with epoxy/TiO_2 NPs respectively. The thickness of epoxy coatings deposited using spin coating technique was calculated through the cross-section image using the field emission scanning electron microscope (FE-SEM) to be about (236 µm), as shown in Fig. 1D.

RESULTS AND DISCUSSION

Structural Characterizations

Field-emission Scanning Electron Microscopy (FE-SEM)

The FE-SEM exam carried out for all prepared laminated samples in order to investigate the morphology and surfaces nature of prepared samples as a function of deposition temperature and TiO_2 NPs addition. Typical morphology view FE-SEM images of Aluminium alloy substrate coated with pure epoxy at different temperatures (25 °C, 50 °C, 75 °C) presented in Fig. 2. From the FE-SEM results observed that the morphology of coated pure epoxy on aluminum alloys substrates as super hydrophobic epoxy coatings exhibited dense micrometer-porous structures of Al substrate type, also observed that the micrometer pores size of deposited pure epoxy on Al substrate are bigger size and less number, this can be attributed

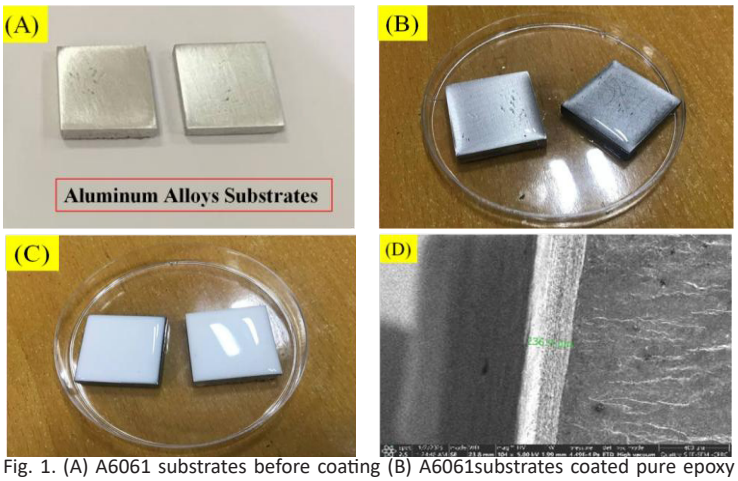

Fig. 1. (A) A6061 substrates before coating (B) A6061substrates coated pure epoxy (C) A6061substrates coated epoxy/TiO_2 NPs (D) cross-section FE-SEM image of epoxy coating on the substrates with thickness about (236 µm)

to higher compatibility of epoxy with the Al alloy substrate as a result of lower rate evolution of hydrogen [26]. On the other hand, observed that the increasing of curing temperature at (75 °C) led to significant decreasing in the number and size of the pores compared to that at (25 °C and 50 °C), which can be attributed to the softening and increasing of the mobility of molecules epoxy at higher curing temperatures. The increase in curing temperature leads to reduce the pores in the epoxy matrix [27,28].

Fig. 3 presents the FE-SEM images of epoxy enhanced TiO_2 NPs coatings at different weight ratios (2, 4 and 6 wt. %) deposited on Al alloy substrate. From the FE-SEM images observed that the adding of TiO_2 NPs to the epoxy matrix led to significantly reduce the porosity structure nature of the epoxy compared with the pure epoxy coatings presented in Fig. 2, where the results showed that the TiO_2 NPs well dispersed within the epoxy porous structure and led to obtained good homogeneous morphology nature of the enhanced epoxy coatings attributed to the TiO_2 NPs occupied the pores within the epoxy structure, as presented in Fig. 3. The FE-SEM images also indicates clear lack of huge pores sizes after the adding of TiO_2 NPs, which confirmed the good dispersion of TiO_2 NPs during the samples preparation procedure. The nano-sizes of the added TiO_2 nanoparticles is a good advantage to be able to penetrate the ultra-small holes, capillary and indentation regions for the metallic Al substrates and the epoxy coatings structure. In the presence of TiO_2 NPs at different ratios (2, 4 and 6 wt. %), the coatings of epoxy nanocomposite demonstrated a textural structure with no agglomeration due to the spherical shapes characteristic of the TiO_2 nanoparticles, as shown in Fig. 3.

X-ray Diffraction (XRD)

The XRD exam carried out to determine the phase type within the prepared laminated samples using spin coating technique. Fig. 4 present the XRD patterns of Al alloys substrates

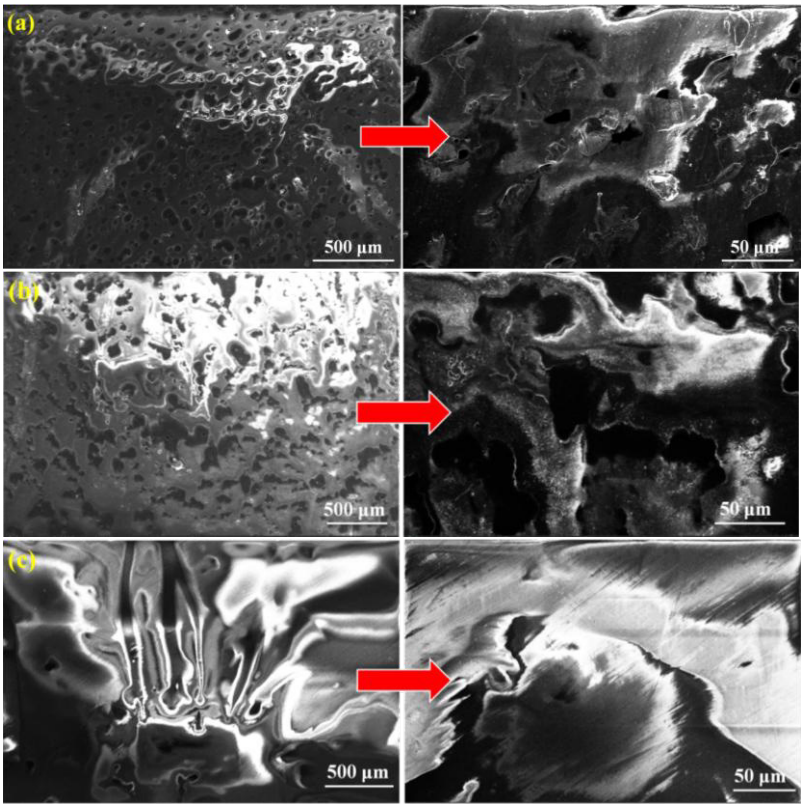

Fig. 2. FE-SEM morphology images of Al alloy substrates deposited epoxy at different curing temperatures (a) at 25 °C (b) at 50 °C (c) at 75 °C

deposited epoxy at different temperatures (25, 50 and 75 °C) respectively, and figure 5 show the XRD patterns of Al alloys substrates deposited epoxy mixed with different weight ratio (2, 4 and 6 wt. %) of titanium oxide nanoparticles TiO_2 NPs respectively. From Figs. 4 and 5 observed there are several characteristic peaks of prepared Al alloy substrates deposited epoxy at (2Θ = 38.46°, 44.71°, 65.09°, 78.22°) with d-spacing (2.3382 A°, 2.0250 A°, 1.4318 A°, 1.2211 A°) of planes (111) (002) (022) (113), these observed peaks assigned to the cubic Al phase within the Al alloy substrates structure with space group (Fm-3m no.225), lattice parameters (a = b = c = 4.0500 A°) and (α = β = γ = 90°) which well matched with the standard data (JCPDS 98-004-3423). While the detected broad characteristic peak centered around (2Θ = 18 °) attributed to the epoxy phase [29]. The XRD patterns of Al alloy substrates deposited epoxy with different ratio of TiO_2 NPs (Fig. 5) showed additional characteristic peaks at (2Θ = 25.41 °, 38.14 °, 48.22 °, 54.34 °, 55.29 °, 63.08 °) with d-spacing (3.5014 A°, 2.3575 A°, 1.8855 A°, 1.6868 A°, 1.6601 A°, 1.4724 A°) of the planes (101) (004) (200) (105) (211) and (204), the detected peaks attributed to the tetragonal TiO_2 phase within the laminated Al alloy substrates structure with space group (I 41/amd no.141), lattice parameters (a = b = 3.7710, c = 9.4300 A°) and (α = β = γ = 90°) which well corresponded with the standard data (JCPDS 96-152-6932).

The obtained XRD results confirmed the presence of all used phases within the prepared samples. The XRD results proved that the increasing of the TiO_2 NPs content within the samples structure as shown in Fig. 5 led to raise the characteristic peaks intensity to be more clear and defined. The XRD results demonstrated that the obtained peaks of all prepared laminated samples slightly shifted from its origin positions with the increasing of temperature and the adding of TiO_2 NPs at different content as shown in

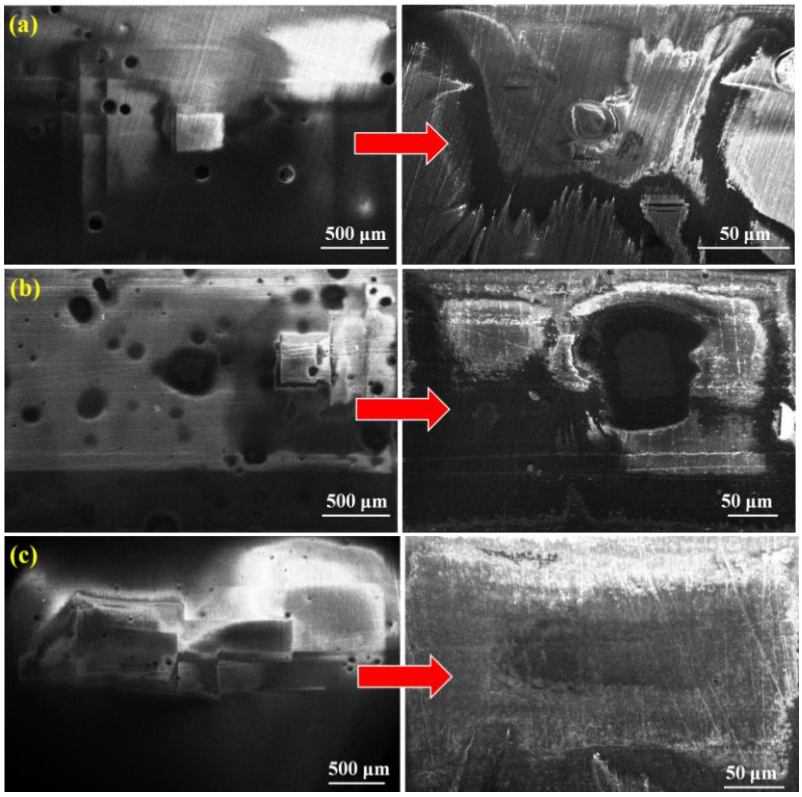

Fig. 3. FE-SEM morphology images of Al alloy substrates deposited epoxy mixed TiO_2 NPs at different ratios (a) 2 wt. % (b) 4 wt. % (c) 6 wt. %

inset plots within the Fig. 5, which indicated the changing of the residual stresses of the laminated prepared samples as a function of temperature and TiO_2 content [30-32].

Energy-dispersive X-ray spectroscopy (EDS)

An elemental examination of the Aluminium alloy substrate 6061 was conducted using Energy Dispersive X-ray Spectroscopy (EDS) to determine the chemical composition and elements ratios within the A 6061 substrate. The obtained EDS results were introduced in two structures: Weight ratio (Wt. %) and Atomic ratio (At %). The aluminum was the predominant component, followed by little amounts of magnesium, iron, chromium, and manganese, as reinforcing elements to enhance the mechanical and corrosion-resistant properties of the Al alloy substrate, Table 1 shown the atomic and weight ratios of Al alloy 6061 substrate elements. Fig. 6 presented the EDS pattern of Al substrate which shows the characteristic peak for each component, responding to the photon energies during electronic transitions. The examination provided evidence for the aluminum

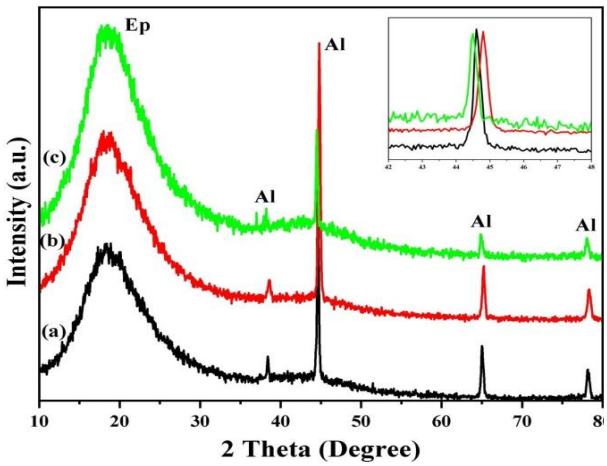

Fig. 4. XRD patterns of Al alloy substrates deposited epoxy at different temperatures (a) 25 °C (b) 50 °C (a) 75 °C.

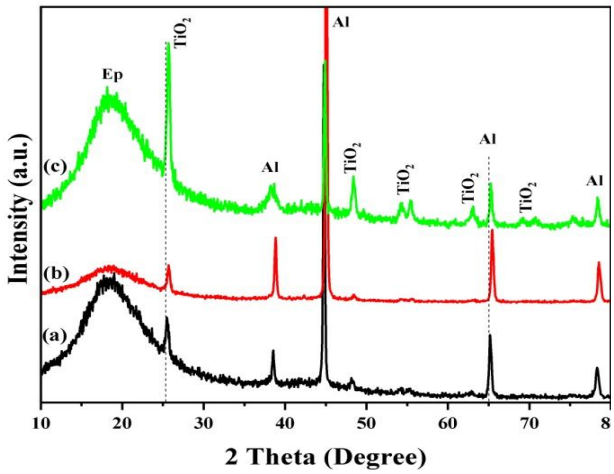

Fig. 5. XRD patterns of Al alloy substrates deposited epoxy mixed with different weight ratio of TiO_2 NPs (a) 2 wt. % (b) 4 wt. % (a) 6 wt. %.

alloy 6061 structure.

Mechanical Properties

Tensile Strength

The measurement of mechanical properties (e.g., elastic modulus and Poisson's ratio) of the epoxy coatings has some difficulties because the structure of epoxy coatings is complex and contains lamellae, pores, micro-cracks. The tensile test achieved to measure the elastic modulus and Poisson's ratio of epoxy coatings. The load is increased continuously with deformation (stress with strain) until failure. Fig. 7 shows the stress-strain curves of the epoxy coatings cured at different temperatures and Fig. 8 shows the stress-strain curves of the epoxy coatings with different TiO_2 NPs ratios. From Fig. 7 observed there is linear elastic response of the stress-strain curves until point of maximum stress followed by suddenly failure at strain larger than (14.52 %) at a temperature 25 °C, (80 %) at 50 °C and (77.6 %) at 75 °C, while for epoxy coatings enhanced different ratios TiO_2 NPs (2, 4 and 6 wt. %) is (25.85 %, 29.6 %, and 64 %) respectively. Elastic modulus was extracted from stress-strain curves curried at various temperatures, while Poison's ratio are determined from longitudinal and lateral strain measured by strain gages during testing. The behavior of all epoxy coatings is similar to metallic materials as indicated in stress-strain curves, i.e. the tensile strength increased with increasing load until failure. Table 2 and 3 are summarized the elastic modulus and Poison's ratio values for epoxy coatings. The epoxy coatins demonstrates higher tensile strength at 25°C compared to 50°C and 75 °C. This is mainly because of how temperature affects the polymer›s molecular structure and its mechanical properties. At lower temperatures, the epoxy's molecular chains move less, making a rigid and strong material. While when the temperature rises, these molecular chains become more mobile, reducing the connections between molecules, therefore lowering tensile strength [33,34]. The observed decrease in epoxy tensile strength at elevated temperatures is linked to enhanced molecular movement. This insight is essential for applications where epoxy materials experience different thermal conditions, as it affects their mechanical performance and how long they last [35,36]. At a curing temperature of 25°C, the tensile strength (T.S) increased by 50%.

The Adding of TiO_2 NPs increased the tensile

Table 1 Chemical composition of Al 6061 alloy substrate.

Element	Atomic %	Atomic % Error	Weight %	Weight % Error
Al	97.4	0.2	97.1	0.2
Mg	0.9	0.0	0.9	0.0
Cr	0.1	0.0	0.2	0.0
Mn	0.1	0.0	0.1	0.0
Fe	0.8	0.0	1.7	0.0

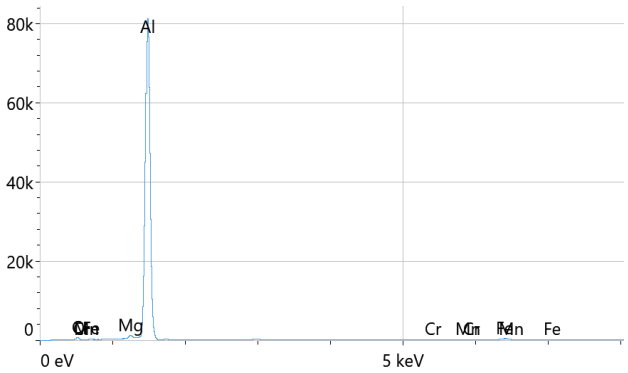

Fig. 6. EDS pattern of used Al 6061 alloy substrate.

strength of epoxy coatings by 25% due to enhanced load transfer at the matrix–particle interface. As showed from Table 4 has higher values of elastic modulus and Poison's ratio due its rigidity because of enhancement by TiO_2 NPs compared to others [37,38]. Observed that the elastic modulus values of epoxy coatings cured at different temperatures are less compared to epoxy coatings enhanced with TiO_2 NPs.

Residual Stresses Calculated Using X-ray Diffraction

The residual stresses of all prepared epoxy coatings samples calculated by the x-ray diffraction technique using the $\sin^2 \Psi$ method. The d-spacing was measured by a diffractometer for different values of Ψ. Fig. 9 presents the obtained curves of $\sin^2 \Psi$ vs. d-spacing for each sample, the slop calculated for all samples, and then the residual stress is obtained using the following relationship [39,40]:

$$\sigma_{\text{res.}} = \frac{\epsilon}{(1+\upsilon)\sin^2 \psi} \frac{d_{\psi - d_n}}{d_n}$$

Where d_ψ is the inter-planar spacing of planes at an angle Ψ to the surface; d_n is the inter-planar spacing of planes normal to the surface; ε is the elastic modulus of the coatings (GPa), ν is Poisson's ratio and Ψ are the angles through which

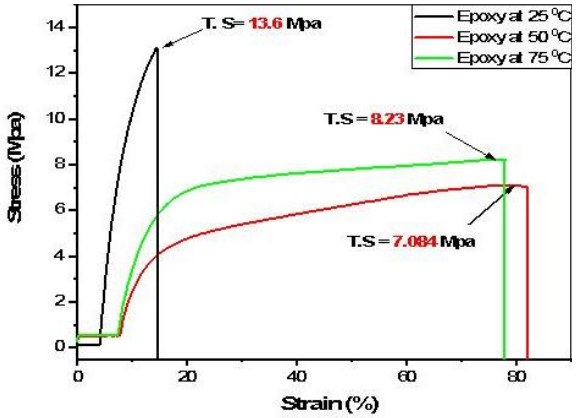

Fig. 7. Stress-strain curves of epoxy coatings at different curing temperature (25, 50 and 75 °C).

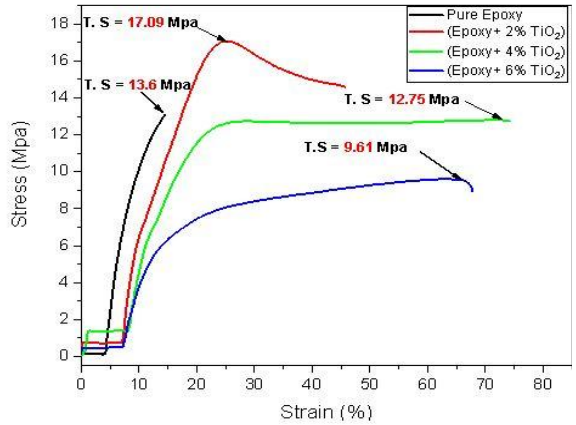

Fig. 8. Stress-strain curves of epoxy coatings with different TiO_2 NPs ratio (2, 4 and 6 wt. %) (At 25 °C).

the sample is rotated.

Table 4 shows the residual stress values obtained through x-ray diffraction using ($\sin^2 \psi$) methods for all prepared laminated samples. The residual stresses values for Al alloy substrate coated epoxy at different temperature (25, 50, and 75 °C) are (−37.64 MPa, −43.89 MPa, and −45.45 MPa) respectively. The obtained results revealed non-linear pattern: the compressive residual stress intensified (became more negative) at 75°C, as shown in Fig. 10.

At curing temperature 25°C, the residual stress indicates limited curing and low cross-linking density, as only partial polymerization occurs at room temperature. As the curing temperature increased to 50°C, the epoxy system entered a more efficient curing stage, increasing the cross-linking density and resulting in a higher compressive residual stress. At 75°C, near-complete curing was achieved, forming a highly cross-linked and rigid polymer network. This led to significant thermal shrinkage during cooling, producing the highest residual compressive stress observed (−45.45 MPa). This shows that there is a significant increase in residual stress values with an increase in curing temperatures of coatings, whereas these values are lower at lower temperatures. It is found from Fig. 10 that the curing temperature 25°C recorded lower value of residual stresses. From these results, it is demonstrated that the residual stresses generated will increase by percentage values of (16.61 and 3.55 %) for epoxy coating when the curing temperature rises from 25 to 75°C. One of the most important properties of epoxy coatings influenced by curing temperature due to the cross-linking density of the epoxy coatings and its process, and this directly affects the values of initiated residual stress. A very dense cross-linking between coating components forms a very strong network through the epoxy coating and enhances its mechanical properties [41]. The Sikadur epoxy system consists of two main components: a base resin, typically based on Bisphenol A diglycidyl ether (DGEBA), and a hardener, usually formulated from various amine compounds such as aliphatic or cycloaliphatic amines. When these two components are mixed, a chemical reaction is initiated between the epoxide functional groups in the resin and the amine groups in the hardener. This reaction leads to the formation of a three-dimensional cross-linking polymer network, where each amine group can react with multiple epoxy groups. The extent and density of these crosslinks—known as the crosslink density—play a fundamental role in determining the final mechanical and physical properties of the cured epoxy. The curing temperature significantly influences the crosslinking process: at low curing temperatures, the reaction progresses slowly, and not all reactive groups fully participate. As a result, the cross-linking density remains relatively low, leading to a softer material with lower mechanical strength. At moderate curing temperatures (50 – 60 °C), the reaction rate increases, resulting in the consumption of more epoxy and amine groups. This results in a denser cross-linking network, improving properties such as hardness, tensile strength, and chemical resistance. At higher curing temperatures (70 °C or above), although cross-linking may initially continue, excessive heat can cause partial degradation of the formed network or volatilization of some reactive components.

Table 2 Elastic modulus and Poisson's ratio of epoxy coatings deposited at different temperatures.

Curing temperature °C	Elastic modulus (MPa)	Poisson's ratio
25	3800	0.302
50	4400	0.313
75	5500	0.319

Table 3 Elastic modulus and Poisson's ratio of epoxy/TiO_2 NPs coatings at different ratios (25 °C).

TiO_2 NPs (wt. %)	Elastic modulus (MPa)	Poisson's ratio
2 %	6400	0.320
4 %	5200	0.322
6 %	4000	0.327

This may limit further cross-linking or even slightly reduce crosslink density if not controlled properly [42].

From Table 4, the obtained results demonstrated that the residual stresses significantly decreased when the TiO_2 NPs added at various ratios (2, 4 and 6 wt. %) compared with the pure epoxy coatings at different temperatures as shown in Fig. 11.

At the TiO_2 NPs ratio (2 wt. %), the residual stressed is slightly reduced to (−31.41 MPa), this decrease is explained by TiO_2 capacity to boost the thermal and mechanical characteristics of the epoxy matrix []. The nanoparticles strengthen the material, aiding in a more even distribution of thermal expansion throughout the coating. The TiO_2 nanoparticles exhibits a low coefficient of thermal expansion (CTE). Incorporating them into the epoxy matrix diminishes the disparity between the epoxy and the substrate, thereby decreasing residual stresses. This aligns with research demonstrating that adding nanoparticles to polymer coatings enhances mechanical

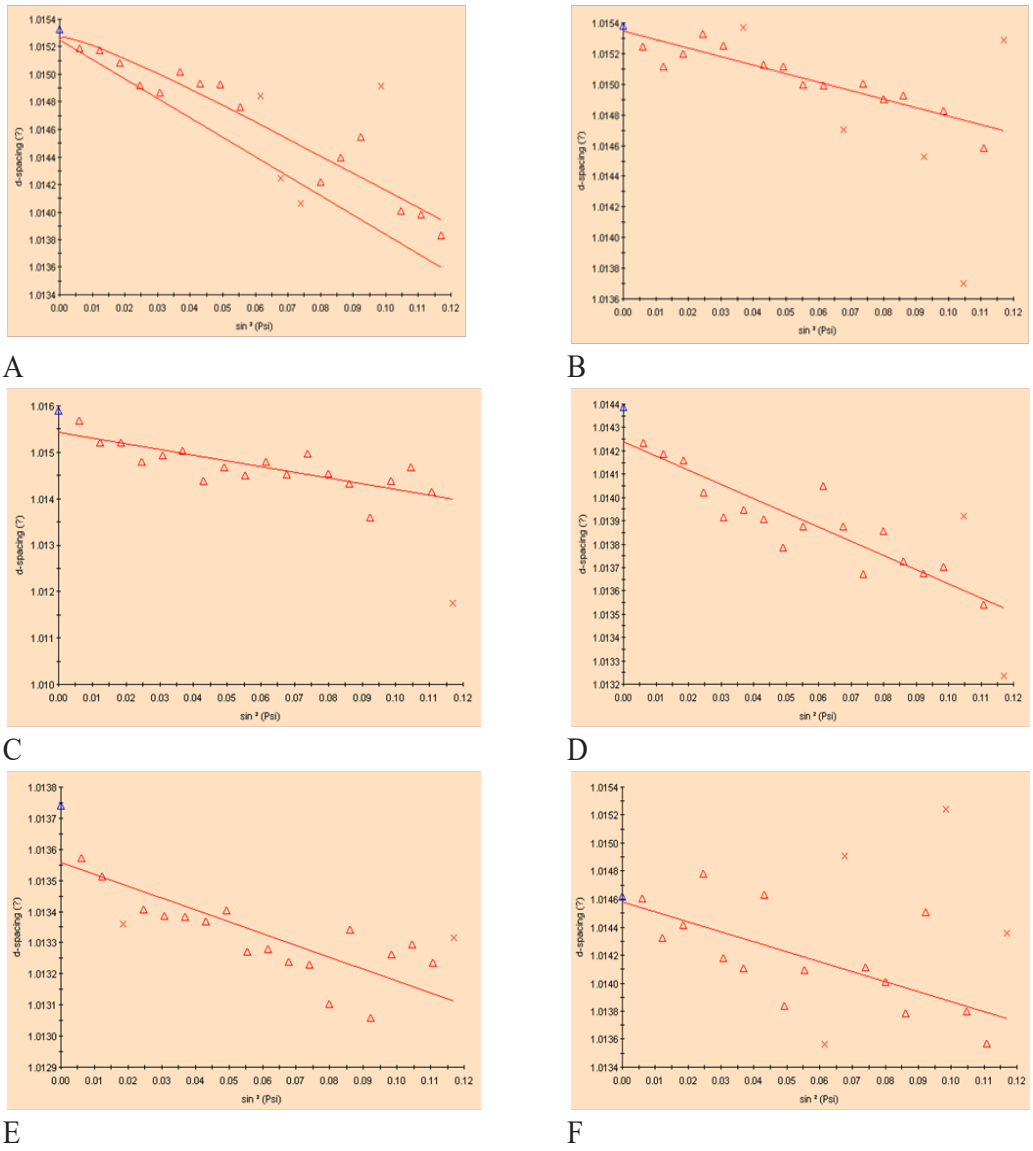

Fig. 9. The $\sin^2 \Psi$ vs. d-spacing curves of Al substrates deposited epoxy (A) Al/epoxy at 25 °C, (B) Al/epoxy at 50 °C, (C) Al/epoxy at 75 °C, (D) Al/epoxy- 2%TiO_2 NPs (E) Al/epoxy- 4%TiO_2 NPs (F) Al/epoxy- 6%TiO_2 NPs.

properties, including stress resistance. With the increase of TiO_2 NPs (4 wt. %) the residual stresses further dropped to (−10.77 MPa), this improvement results from the efficient dispersion of TiO_2 particles within the epoxy matrix. As the TiO_2 concentration rises to this point, it

Table 4 Residual Stresses values for all prepared epoxy coatings.

Sample	Residual Stress (MPa)
Al alloy/Ep at 25 °C	-37.64
Al alloy/Ep at 50 °C	-43.89
Al alloy/Ep at 75 °C	-45.45
Al alloy/Ep- 2 % TiO_2	-31.41
Al alloy/Ep- 4 % TiO_2	-10.77
Al alloy/Ep- 6 % TiO_2	-19.80

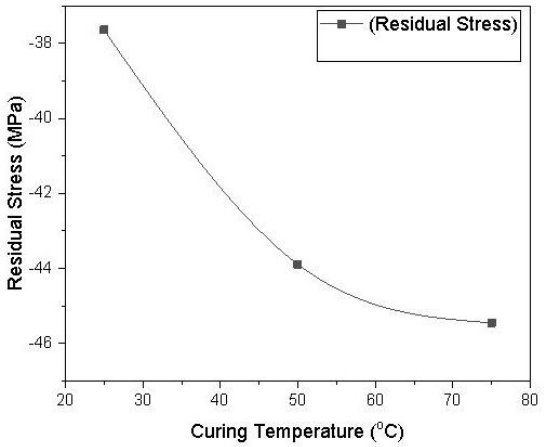

Fig. .10. the variation of residual stresses of epoxy coatings cured at different temperatures (25, 50 and 75 °C).

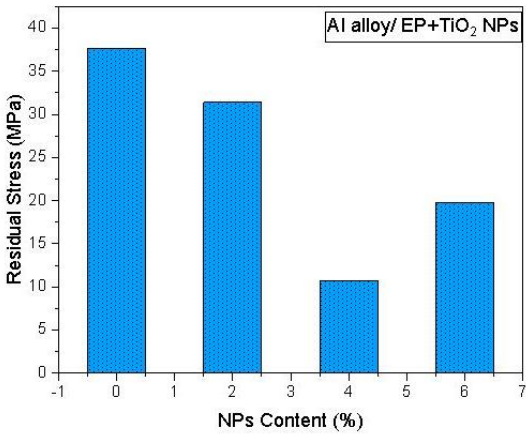

Fig. 11. the variation of residual stresses of epoxy coatings with different TiO_2 NPs ratios (2, 4 and 6wt. %).

reinforces the structure more evenly, leading to an additional decrease in the residual stress. Adding TiO_2 helps minimize the thermal expansion mismatch between the epoxy and the aluminum substrate, a major contributor to residual stress in coated materials [43-45]. The even distribution of nanoparticles further stabilizes the thermal properties of the nanocomposites, resulting in a significant reduction in residual stresses. This concentration represents the optimal loading level, where the TiO_2 NPs well dispersed within the epoxy matrix.

The residual stresses at higher TiO_2 NPs ratio (6 wt. %) indicated partial re-increasing (−19.80 MPa); the rise in residual stresses may be attributed to several factors. At this higher concentration, the TiO_2 NPs might not be evenly distributed throughout the epoxy matrix, which can form stresses concentrations. Furthermore, adding more TiO_2 NPs can increase the epoxy viscosity, possibly causing poor wetting and adhesion between the TiO_2 NPs and the polymeric matrix. This unevenness can create internal stresses because of an incomplete interaction between the epoxy and the reinforcing material [37]. The increase in residual stress at this concentration corresponds with previous studies suggesting that excessive nanoparticle loading can lead to clumping and ineffective stress distribution [38]. In general, in this research residual stresses are reduced by adding nanoparticles at the same curing temperature (25 °C).

CONCLUSION

This work reports the successful preparation of the distinctive laminated Aluminum/epoxy-TiO_2 NPs composites using the simple, easy and effective spin coating technique, as well as using non-destructive x-ray technique to estimate the residual stresses of the laminated samples. The results revealed that the curing temperature and the adding of TiO_2 NPs exhibited significant effect on the residual stresses values. The Al alloy/epoxy cured at (25 °C) recorded the lowest compressive residual stresses value (-37.64 MPa), with the increase of curing temperature of (50 and 75 °C) led to raise the values of residual stresses. The adding of TiO_2 NPs to epoxy coatings indicated obvious decrease in the residual stresses values compared with the pure epoxy coating cured at (25 °C). The Al alloy/epoxy- 4 wt. % TiO_2 NPs recorded lowest residual stresses value to be (-10.77 MPa), and (-31.41 and -19.8 MPa) at TiO_2 NPs ratios (2 and 6 wt. %) respectively. At high TiO_2 NPs ratio (6 wt. %) led to increase the residual stresses values due to the TiO_2 NPs may forms stresses concentrations and poor wetting ratio between the nanoparticles and the matrix. The obtained results proved that the prepared epoxy coatings have high potential to be suitable candidates to apply as wear protection epoxy coatings in many advanced applications, especially in the oil sector in coating the oil pipelines and tanks, and the aircraft field.

CONFLICT OF INTEREST

The authors declare that there is no conflict of interests regarding the publication of this manuscript.

REFERENCES

1. Wisnom MR, Gigliotti M, Ersoy N, Campbell M, Potter KD. Mechanisms generating residual stresses and distortion during manufacture of polymer–matrix composite structures. Composites Part A: Applied Science and Manufacturing. 2006;37(4):522-529.
2. George M, Coupeau C, Colin J, Grilhé J. Mechanical behaviour of metallic thin films on polymeric substrates and the effect of ion beam assistance on crack propagation. Acta Mater. 2005;53(2):411-417.
3. Marx VM, Toth F, Wiesinger A, Berger J, Kirchlechner C, Cordill MJ, et al. The influence of a brittle Cr interlayer on the deformation behavior of thin Cu films on flexible substrates: Experiment and model. Acta Mater. 2015;89:278-289.
4. Al-Timimi MH, Albanda WH, Abdullah MZ. Influence of Thickness on Some Physical Characterization for Nanostructured MgO Thin Films. East European Journal of Physics. 2023(2):173-181.
5. Coupeau C. Atomic force microscopy study of the morphological shape of thin film buckling. Thin Solid Films. 2002;406(1-2):190-194.
6. Moon MW, Chung JW, Lee KR, Oh KH, Wang R, Evans AG. An experimental study of the influence of imperfections on the buckling of compressed thin films. Acta Mater. 2002;50(5):1219-1227.
7. Bemporad E, Sebastiani M, Casadei F, Carassiti F. Modelling, production and characterisation of duplex coatings (HVOF and PVD) on Ti–6Al–4V substrate for specific mechanical applications. Surf Coat Technol. 2007;201(18):7652-7662.
8. Schmidt S, Hänninen T, Wissting J, Hultman L, Goebbels N, Santana A, et al. SiNx coatings deposited by reactive high power impulse magnetron sputtering: Process parameters influencing the residual coating stress. J Appl Phys. 2017;121(17).
9. Chang J-Y, Yu G-P, Huang J-H. Determination of Young's modulus and Poisson's ratio of thin films by combining sin2ψ X-ray diffraction and laser curvature methods. Thin Solid Films. 2009;517(24):6759-6766.
10. Sobol' OV, Andreev AA, Grigoriev SN, Volosova MA, Gorban' VF. Vacuum-arc multilayer nanostructured TiN/Ti coatings: structure, stress state, properties. Met Sci Heat Treat. 2012;54(1-2):28-33.
11. Metel A, Grigoriev S, Melnik Y, Panin V, Prudnikov V. Cutting

Tools Nitriding in Plasma Produced by a Fast Neutral Molecule Beam. Jpn J Appl Phys. 2011;50(8S1):08JG04.
12. Fominski VY, Grigoriev SN, Celis JP, Romanov RI, Oshurko VB. Structure and mechanical properties of W–Se–C/diamond-like carbon and W–Se/diamond-like carbon bi-layer coatings prepared by pulsed laser deposition. Thin Solid Films. 2012;520(21):6476-6483.
13. Vereschaka AS, Grigoriev SN, Tabakov VP, Sotova ES, Vereschaka AA, Kulikov MY. Improving the Efficiency of the Cutting Tool Made of Ceramic when Machining Hardened Steel by Applying Nano-Dispersed Multi-Layered Coatings. Key Eng Mater. 2013;581:68-73.
14. Vereschaka AA, Vereschaka AS, Grigoriev SN, Kirillov AK, Khaustova OU. Development and Research of Environmentally Friendly Dry Technological Machining System with Compensation of Physical Function of Cutting Fluids. Procedia CIRP. 2013;7:311-316.
15. Jagannadham K, Watkins TR. A Comparative Study of Residual Stresses in Single and Multilayer Composite Diamond Coatings. MRS Proceedings. 1997;505.
16. Antonucci V, Cusano A, Giordano M, Nasser J, Nicolais L. Cure-induced residual strain build-up in a thermoset resin. Composites Part A: Applied Science and Manufacturing. 2006;37(4):592-601.
17. Soliman TS, Abomostafa HM, Abouhaswa AS. Synthesis of $Ni_{0.8}Mg_{0.2}Fe_2O_4$ nanoparticles and its impact in enhancing the structural, magnetic, and optical properties of the PVA-CMC polymer blend. Inorg Chem Commun. 2024;164:112408.
18. Ayoub RH, Al-Timimi MH, Abdullah MZ. Enhancements of Structural and Optical Properties of MgO: SnO_2 Nanostructure Films. East European Journal of Physics. 2023(3):546-554.
19. Abadias G, Chason E, Keckes J, Sebastiani M, Thompson GB, Barthel E, et al. Review Article: Stress in thin films and coatings: Current status, challenges, and prospects. Journal of Vacuum Science and Technology A: Vacuum, Surfaces, and Films. 2018;36(2).
20. Hadi JH. Investigation of residual stress in epoxy-based coatings using X-ray and FEM-ANN techniques. Ministry of Science and Technology, Vietnam. 2023;65(4):54-61.
21. Holdway P, Bowen AW. Surface and Near-Surface Analysis of Residual Stresses in Aluminium and Titanium Alloys — Examples of the Case for X-Ray Diffraction. Measurement of Residual and Applied Stress Using Neutron Diffraction: Springer Netherlands; 1992. p. 461-471.
22. Taisei D, Nishida M, Junichi O. Residual Stress Measurement of Industrial Polymers by X-Ray Diffraction. Advanced Materials Research. 2015;1110:100-103.
23. Al-Jaafari MAA. Study the Effects of Titanium Dioxide nano particles reinforcement on the mechanical properties of Aluminum Alloys composite. IOP Conference Series: Materials Science and Engineering. 2021;1105(1):012062.
24. Samah RH, Mudhar AA-O, Hamid MM, Sergey K. Residual Stresses Characterisation of Hard Ceramic Coating (SiC-5wt%Al_2O_3) Using X-Ray Diffraction Technique. Journal of Techniques. 2024;6(3):35-40.
25. Test Method for Verifying the Alignment of X-Ray Diffraction Instrumentation for Residual Stress Measurement. ASTM International.
26. Mišković-Stanković VB, Stanić MR, Dražić DM. Corrosion protection of aluminium by a cataphoretic epoxy coating. Prog Org Coat. 1999;36(1-2):53-63.
27. Khotbehsara MM, Manalo A, Aravinthan T, Reddy KR, Ferdous W, Wong H, et al. Effect of elevated in-service temperature on the mechanical properties and microstructure of particulate-filled epoxy polymers. Polymer Degradation and Stability. 2019;170:108994.
28. Mawat AJ, Al-Timimi MH, Albanda WH, Abdullah MZ. Morphological and optical properties of $Mg_{1-x}CdS_x$ nanostructured thin films. AIP Conference Proceedings: AIP Publishing; 2023. p. 090019.
29. Singh SK, Singh TJ, Nayak B, Sonker PK, Singh MA. Analysis of the impact of exfoliated graphene oxide on the mechanical performance and in-plane fracture resistance of epoxy-based nanocomposite. High Perform Polym. 2024;36(9-10):487-507.
30. Shokrieh MM, Daneshvar A, Akbari S. Reduction of thermal residual stresses of laminated polymer composites by addition of carbon nanotubes. Materials and Design. 2014;53:209-216.
31. Kim SS, Murayama H, Kageyama K, Uzawa K, Kanai M. Study on the curing process for carbon/epoxy composites to reduce thermal residual stress. Composites Part A: Applied Science and Manufacturing. 2012;43(8):1197-1202.
32. Rahayu I, Noviyanti AR, Rakhmawaty D, Anggraeni A, Bahti HH, Hidayat S, et al. Preparation of Lithium Iron Phosphate-Carbon Composite as a Cathode for Lithium Ion Battery. Mater Sci Forum. 2019;966:392-397.
33. Balan AE, Al-Sharea A, Lavasani EJ, Tanasa E, Voinea S, Dobrica B, et al. Paraffin-Multilayer Graphene Composite for Thermal Management in Electronics. Materials. 2023;16(6):2310.
34. Banea MD, Silva LFMd, Campilho RDSG. Effect of Temperature on Tensile Strength and Mode I Fracture Toughness of a High Temperature Epoxy Adhesive. J Adhes Sci Technol. 2012;26(7):939-953.
35. Lan Z, Deng J, Xu Z, Ye Z, Nie Y. Study of Heat Treatment Effect on Mechanical Properties of Epoxy Resin Reinforced with Fiber Glass. Polymers. 2023;15(12):2734.
36. Banea MD, de Sousa FSM, da Silva LFM, Campilho RDSG, de Pereira AMB. Effects of Temperature and Loading Rate on the Mechanical Properties of a High Temperature Epoxy Adhesive. J Adhes Sci Technol. 2011;25(18):2461-2474.
37. Srinivasa Perumal KP, Selvarajan L, Mathan Kumar P, Shriguppikar S. Enhancing mechanical and morphological properties of glass fiber reinforced epoxy polymer composites through rutile nanoparticle incorporation. Progress in Additive Manufacturing. 2024;10(1):831-848.
38. Nguyen TA, Nguyen TH, Nguyen TV, Thai H, Shi X. Effect of Nanoparticles on the Thermal and Mechanical Properties of Epoxy Coatings. Journal of Nanoscience and Nanotechnology. 2016;16(9):9874-9881.
39. Residual Stress Measurement by X-Ray Diffraction. SAE International.
40. Gazzara CP. X-Ray Residual Stress Measurement Systems for Army Material Problems. Residual Stress and Stress Relaxation: Springer US; 1982. p. 369-388.
41. Sharma J, Kumar Arya R, Verros GD. A comprehensive model for the drying of glassy polymer coatings: The low solvent concentration area of the system poly(styrene)/P-xylene. Prog Org Coat. 2019;135:622-628.
42. Li X, Zhang X, Chen J, Huang L, Lv Y. Uniaxial Tensile Creep Behavior of Epoxy-Based Polymer Using Molecular Simulation. Polymers. 2021;13(2):261.
43. Chan EP, Kundu S, Lin Q, Stafford CM. Quantifying the Stress Relaxation Modulus of Polymer Thin Films via Thermal Wrinkling. ACS Applied Materials and Interfaces. 2010;3(2):331-338.
44. Ahmed G, Ahmed G. Coclosed Rickart Modules. Ibn AL-Haitham Journal For Pure and Applied Sciences. 2018:452-462.
45. Synthesis, Characterization and Biological Activity of Zinc Oxide Nanoparticles (ZnO NPs) Asmaa H. Hammadi, S.Abdulmunem Habeeb, Lena Fadhil Al-Jibouri, Falah H. Hussien. Systematic Reviews in Pharmacy. 2020;11(05).